Journal Name

ARTICLE TYPE

Cite this: DOI: 10.1039/xxxxxxxxxx

Discrimination between hydrogen bonding and protonation in the spectra of a surface-enhanced Raman sensor†

Nungnit Wattanavichean, Ella Casey, Richard J. Nichols and Heike Arnolds*

Received Date
Accepted Date

DOI: 10.1039/xxxxxxxxxx

www.rsc.org/journalname

We investigate the surface-enhanced Raman spectra of 4-mercaptopyridine on gold in a variety of acids. 4-mercaptopyridine is a known pH sensor which exhibits characteristic spectral changes when the pH is changed. Here we show with the help of experiment and density functional calculations that the ring breathing mode is also highly sensitive to hydrogen bonding. Its spectral signature is a broad band with up to three contributions from free, protonated and hydrogen-bonded 4-mercaptopyridine. Unlike pyridine in solution, where protonation leads to a higher ring breathing frequency than hydrogen-bonding, we find that protonated adsorbed 4-mercaptopyridine possesses a frequency which is lower than the corresponding hydrogen-bonded species. The Raman spectra indicate an orientation change of the aromatic ring in acidic solutions, which could be caused by a cation/π interaction between protonated and deprotonated 4-mercaptopyridine. As the frequencies of the three species are well separated, adsorbed 4-mercaptopyridine can probe more complex changes in the solution environment than just pH.

1 Introduction

The interest in 4-mercaptopyridine (pyS) as an adsorbate and sensor arises from a wide range of scientific areas, encompassing its use as electron transfer promotor in bioelectrochemistry[1], as sensor of protons and metal ions[2,3] and in the construction of metal-molecule junctions in molecular electronics[4]. These applications arise from its self-assembly on noble metal surfaces via the thiol group, which exposes the nitrogen lone pair to the solution and makes it available for coordination to metal ions or protons. In recent years, this basic concept has also been extended to a variety of pyridine-terminated self-assembled monolayers (SAMs) with improved self-assembly and electron transfer properties[5,6]. These various applications have been furthered by the strong Raman response of the highly polarisable pyridine ring, which permits the facile detection of small amounts of pyS by surface-enhanced Raman spectroscopy (SERS)[7]. Together with characteristic pH-dependent changes, particularly in the ring-breathing and ring-stretching regions[8,9], this has enabled pH sensing inside living cells with pyS adsorbed on noble metal nanoparticles[10,11]. Recently, these spectral signatures have also been used for enantioselective detection of alcohols via hydrogen bonding, through an orientation-dependent charge-transfer effect[12].

All these studies are based on observing changes in the ratios of several pH-sensitive peak pairs. The C=C stretch frequency of the ring is a reliable indicator of proton transfer, as it changes significantly from $\approx$ 1580 cm^{-1} to $\approx$ 1610 cm^{-1} upon protonation. More common though is to employ the intensity ratio of ring breathing and trigonal ring deformation peaks at $\approx$ 1000 cm^{-1} and $\approx$ 1100 cm^{-1}, respectively, since these are the most intense for all excitation wavelengths[7]. Protonation stabilises the aromatic ring, which increases the ring breathing intensity. At the same time, the double-bond character of the C-S bond involved in the trigonal ring deformation is decreased, which decreases its intensity.

Despite the widespread use of 4-mercaptopyridine as a pH sensor, the reported spectral changes which occur on protonation and the peaks used for pH determination vary considerably in the available literature[11,13]. This might relate to incomplete understanding of what determines the pKa of adsorbed pyS, with reported values of 4.6[14], 5.3[13] and 7.5[15]. Discrepancies could also arise because the current literature makes no distinction between protonation of, or hydrogen bonding to 4-mercaptopyridine. This is surprising, given that the ring-breathing frequency of pyridine has been shown to vary by several wavenumbers between free, hydrogen-bonded and protonated species[16].

Department of Chemistry, University of Liverpool, Crown Street, Liverpool L69 7ZD, UK. E-mail: heike.arnolds@liverpool.ac.uk

† Electronic Supplementary Information (ESI) available: Additional Raman spectra, including examples of background subtraction and normalisation. Density Functional Theory results, including verification of calculated spectra, frequencies and geometric parameters of calculated molecules. See DOI: 10.1039/b000000x/

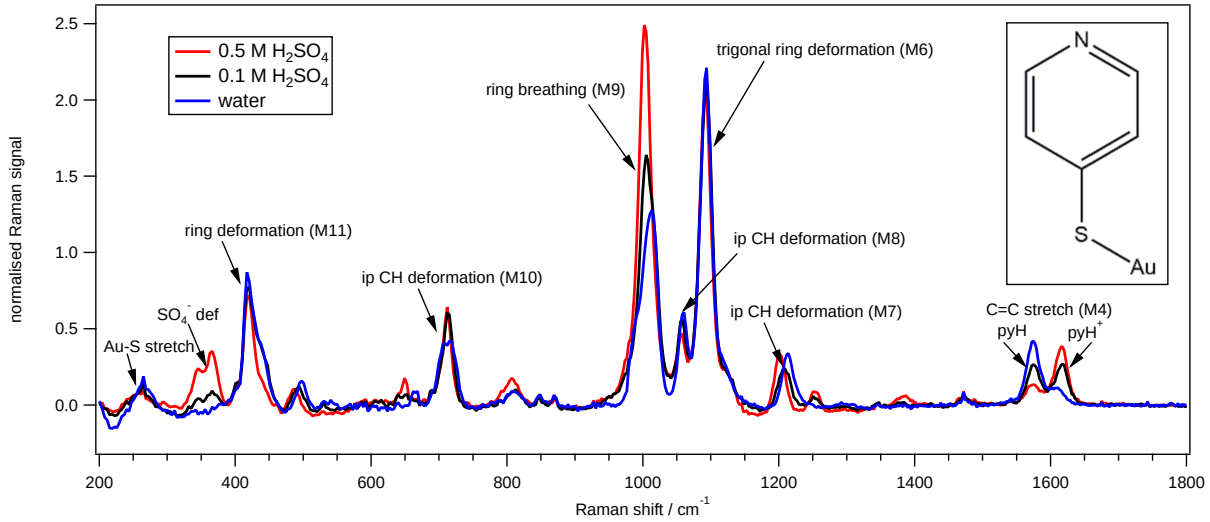

Fig. 1 Typical Raman spectra of pyS-Au (shown in the inset) on roughened gold in ultrapure water and 0.1 and 0.5 M H_2SO_4 .

Here we show that adsorbed pyS likewise exists as free, hydrogen-bonded and protonated species, which can be distinguished by their ring-breathing frequency. We identify the corresponding characteristic frequencies by analysing the surface-enhanced Raman spectra of 4-mercaptopyridine on roughened gold and gold nanoparticles in a variety of acids. Unlike pyridine in solution, we find that the protonated species has a lower ring breathing frequency than the hydrogen bonded one. From a detailed analysis of the spectra and comparison with density functional theory (DFT) results, we identify an orientation change of the ring as the likely explanation.

2 Experimental

2.1 Gold substrate preparation

Polycrystalline gold foil (99.95 % purity) (Advent Research Materials) was electrochemically roughened according to Tian *et al.* and Li *et al.*[17,18] in 0.1 M KCl, by holding the potential at first at -1.16 V vs SCE for 10 min and stepping to -0.06 V vs SCE for 2 min. The potential was then swept from -0.06 to 1.44 V and back for 20 oxidation-reduction cycles at 750 mV/s. During each cycle, the potential was held at -0.06 V vs SCE for 30 s and then at 1.44 V vs SCE for 2 s. Finally, the potential was held at -0.36 V vs SCE for 2 min to desorb any adsorbed Cl^- ions and the gold electrode was rinsed thoroughly with ultrapure (18 MΩ) water. To remove pyS, the sample was run as a working electrode with a gold counter electrode and Ag/AgCl reference electrode in 0.1 M NaOH. 20 cycles were run over a potential range between -1.2 to +1.4 V vs SCE at a scan rate of 10 mV/s[19]. For comparison, we also prepared 50 nm gold nanoparticles with thin silica shell[20], which were dried on clean silicon wafers. Presence of the shell avoided aggregation by bridging pyS and pinholes allowed for adsorption.

2.2 Mercaptopyridine adsorption

We used 4,4′-dipyridyl disulfide (Aldrithiol-4, 98 % purity) as supplied by Sigma-Aldrich (Poole, UK). A 40 μM solution was prepared in hot, ultrapure water and the sample typically left for 15 - 30 minutes at room temperature. The sample was removed from solution, rinsed with ultrapure water and dried under a stream of nitrogen or argon. All acids were analytical grade. The SERS spectra of the sample were measured immersed in various acids.

2.3 Raman characterisation

Raman spectroscopy was carried out using a MiniRam II (B&W Tek, USA) with BWSpec software. The MiniRam II uses a 785 nm diode laser and has a spectral resolution of 10 cm^{-1} . The laser power was typically between 150 mW and 300 mW with a focal point diameter of 75 μm, corresponding to an intensity of 3.4×10^7 W m^{-2}. Typical accumulation time was between 30 s and 65 s. Spectra were normalised to the background intensity in a region without peaks (750 cm^{-1} , arbitrary choice) because peak height is proportional to background height, which in turn is a measure for the Raman enhancement factor (see supporting information, Figure S1). For better spectral deconvolution of the ring breathing mode, we subtract a polynomial from the spectra using IgorPro from Wavemetrics. The raw and normalised spectra are shown in the supporting information (Figure S2).

2.4 Calculations

DFT calculation of Raman spectra was carried out with Spartan 16 software, using density functional theory with the B3LYP hybrid functional with 6-31G** basis set. This was found to give good agreement in the calculation of Raman spectra of thymine[21], while performing reasonably well in the calculation of dissociation energies of hydrogen-bonded species[22]. With a single metal atom, this level of DFT reproduces the frequencies calculated by Birke and Lombardi for pyS on silver[23] very well, with the exception of the metal-molecule stretch (see supporting information, Figures S3 and S4).

3 Results and discussion

The Raman spectra of pyS in ultrapure water and sulfuric acid are shown in Figure 1. Peaks have been labelled with the notation by Gardner and Wright[24] for monosubstituted benzenes, following a recent assignment by Birke and Lombardi[23]. All the major visible peaks are totally symmetric with respect to the C_{2v} axis of the pyridine ring, as expected for SERS. A small number of other peaks are visible: out-of-plane deformation of the ring at 497 cm^{-1} (mode $\mathscr{M}19$, b_1 symmetry); in-plane asymmetric ring deformation of the ring at 662 cm^{-1} ($\mathscr{M}29$, b_2 symmetry); out-of-plane CH + ring deformation at 810 cm^{-1} ($\mathscr{M}17$, b_1 symmetry). While the appearance of such peaks is often interpreted as presence of charge transfer enhancement in SERS, a far simpler explanation lies in the symmetry of the adsorbate. If the pyridine ring plane and/or the ring edge is tilted towards the surface, as sketched in Figure 2, the overall symmetry of the adsorbate is only C_s. Depending on the orientation of the mirror plane, either in-plane (b_2) or out-of-plane (b_1) modes become totally symmetric. On these rough surfaces, a large spread of orientations can be expected, so it is neither surprising that peaks of lower symmetry vibrations appear, nor is it necessarily an indication of additional charge transfer enhancement.

Protonation affects several Raman peaks as seen in Figure 1. The largest frequency shift occurs for the C=C stretch, which is found at ≈ 1580 cm^{-1} for pyS-Au and at ≈ 1610 cm^{-1} for H^+-pyS-Au[9,13,25–28]. The intensity ratio of these two peaks is therefore often used to determine the local pH. The ring breathing peak gains in intensity as expected, although the intensity of the trigonal ring deformation shows a small increase instead of the expected decrease. The symmetric in-plane C-H bending mode shifts from 1214 cm^{-1} in water down to 1206 cm^{-1} in acid. The protonated adsorbate layer also always shows a small peak at 1250 cm^{-1}. This is most likely mode $\mathscr{M}25$, an asymmetric in-plane C-H bend, so its appearance could indicate a change in the orientation of pyS upon protonation.

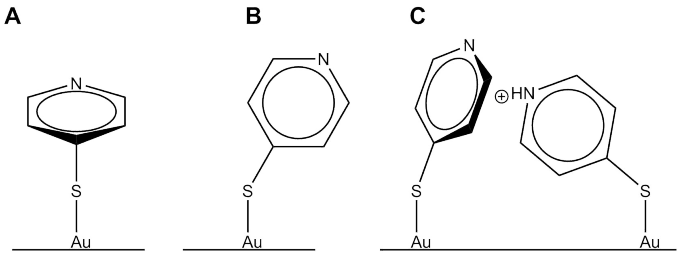

Fig. 2 Sketch of possible orientations of pyS-Au. A: pyridine ring plane tilted towards surface (out-of-plane modes become totally symmetric); B: edge of pyridine ring tilted towards surface (in-plane modes become totally symmetric); C: potential cation/π interaction between neutral and protonated pyridine rings on the surface.

The pH-dependent changes have all been described in the prior literature, with the exception of the remarkable change in the shape of the ring breathing mode in Figure 1. Generally, it is relatively narrow in highly acidic solution and appears to develop shoulders on its low and high frequency sides in neutral or basic solution (see supporting information Figure S5 for additional spectra). In order to unravel the origin of the three components, we fit the ring breathing region of the spectra in Fig. 1 with three Gaussians in a global fit, which restricts the two higher frequency components to be at the same frequency for all three spectra. The results are shown in detail in Fig. 3.

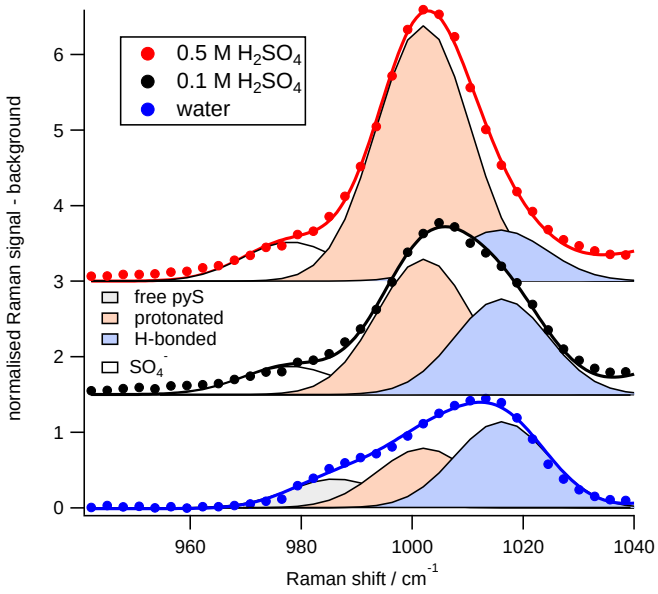

Fig. 3 The ring breathing region of Au-pyS spectra in water and diluted H_2SO_4 can be fitted with three Gaussians.

The common peaks in the three spectra are found at 1002.1 cm^{-1} and 1016.1 cm^{-1}. We also fitted a low frequency shoulder with solvent-dependent frequency. In water, this shoulder is at the expected frequency for free pyS, 986.1 cm^{-1}. The peak in H_2SO_4 at 978.0 cm^{-1} corresponds to a vibrational mode of the sulfate anion, which is the only adsorbed species found on metal electrodes[29,30]. Figure 3 shows how the highest frequency component decreases in height as we change from water to more concentrated acid. We therefore propose that the three peaks correspond to three different species of adsorbed mercaptopyridine, namely pyS-Au at 986.5 cm^{-1}, H^+-pyS-Au at 1002.1 cm^{-1} and $H_2O\cdots$pyS-Au at 1016.1 cm^{-1}.

Hydrogen bonding is known to affect the frequency of the pyridine ring breathing mode[16]: free pyridine has a ring breathing mode at 990 cm^{-1}, hydrogen-bonded pyridine vibrates at 994 cm^{-1} and protonated pyridine has a ring breathing frequency of 1003 cm^{-1}. The blue shift of the frequency indicates stronger bonds and thereby a more stable aromatic ring. This can be explained in an intuitive way: the stability increases because H-bonding pulls the electron density of the nitrogen lone pair away from the aromatic ring system. Therefore, the delocalised π-electrons in the pyridine ring are less disturbed by the lone pair electrons. The shorter the hydrogen bond, the more stable the aromatic ring; a trend which is continued for H^+-py, which is still aromatic, since the proton binds to the lone pair and not the ring. A more sophisticated model[31,32] uses the concept of hyperconjugation. Some of the lone pair electron density resides in an antibonding orbital of the C_2-C_3 and C_5-C_6 σ bonds. Hydro-

gen bonding or protonation removes some of this electron density, thereby strengthening the ring. This can be recognised by a shortening of the C_2-C_3 and C_5-C_6 bonds in pyridine[33]. The thiol group in pyS is an electron donating group, which increases the basicity and therefore electron donating capability of the lone pair, so in principle one would expect a similar frequency ordering as for pyridine itself, but a larger frequency shift. However, in Fig. 3, it is clearly the central peak at 1002.0 cm^{-1} whose intensity correlates with the increasing acid concentration, not the highest frequency peak.

As this result is unexpected and SERS studies can sometimes suffer from poor reproducibility due to the highly inhomogeneous nature of the substrate, we analysed 25 pyS spectra on both roughened gold as well as nanoparticles in a variety of solvents (H_2SO_4, NaOH, phosphate buffered saline and H_2O for rough gold, H_2SO_4, $HClO_4$, acetic acid and HCl for nanoparticles), fitting the ring breathing region with three peaks and comparing the ratio of the acid peak area around 1002 cm^{-1} versus the sum of the areas of the free and hydrogen bonded pyS to the established ratio of protonated C=C stretch at 1610 cm^{-1} versus deprotonated C=C stretch at 1580 cm^{-1}. The result is shown as a scatter plot in Fig. 4, while details of conditions and fitting results can be found in the supporting information (Table S1). Different ratios for the same acid or base arise from different concentrations, while different ratios for water are caused by variations in coverage or whether the sample was exposed to acid or base beforehand. A strong positive correlation can be seen (Pearson's coefficient = 0.85) which confirms our assignment from Fig. 3.

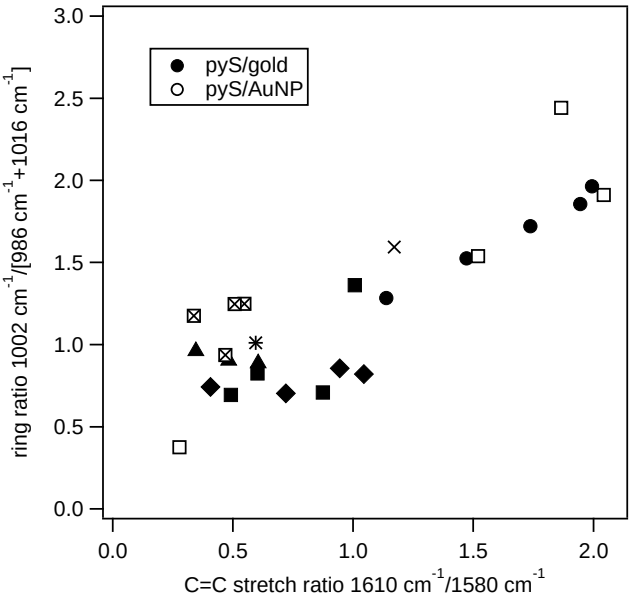

Fig. 4 Ratio of ring breathing versus ratio of ring stretching peaks for pyS adsorbed on rough gold (filled symbols) and SHINs (open symbols). ◯ H_2SO_4; □ water; ◊ buffer; △ NaOH; × acetic acid; ∗ HCl; ⊠ $HClO_4$.

The unusual order of the ring breathing frequencies of ν(pyS-Au)< ν(H^+-pyS-Au)< ν($H_2O\cdots$pyS-Au) could possibly be explained by an orientation change of the ring. Protonation creates a cation, which could undergo a cation/π interaction with a neighbouring neutral adsorbate. For example, the interaction energy between protonated pyridine and benzene is highest for a T-shaped conformation[34]. This interaction would not occur in the bulk, where the protonation of pyridine leads to homodimer formation with a symmetric N···H···N bond[35]. On the surface though, as sketched in Figure 2C, the range of possible geometries is limited by the bond to the surface, which could make a tilting of protonated adsorbed pyS towards the ring of neutral adsorbed pyS more favourable (typical distances between adsorbed molecules are 3 to 5 Å in ordered layers on Au(111)[36]).

Very little is known experimentally about the adsorption site and orientation of 4-mercaptopyridine on gold. The now generally accepted model for thiol adsorption on gold surfaces is one of "gold mining", where the gold-thiol interaction leads to the formation of supersurface Au atoms with two attached thiols[37]. This is consistent with scanning tunneling microscopy (STM) studies of adsorbed mercaptopyridine in perchloric acid solutions, which suggested that the molecules are adsorbed in pairs with close proximity of sulfur adatoms, resembling a pySSpy dimer[38,39]. Thiols adsorbed on small gold clusters have been shown to form Au-SR-Au-SR-Au staple motifs[40], which resemble the bridge adsorption site predicted by DFT for pyS on Au(111)[41]. The same DFT study found that protonation weakens the interaction with the surface and reduces the energetic preference for bridge versus atop site which indicates that protonated pyS could rearrange more easily. Single coordination to gold, as expected in the gold mining model, would result in larger conformational freedom and easier reorientation on protonation.

There are several indicators in our Raman spectra for a change in the configuration of adsorbed mercaptopyridine at low pH, even though some of the relevant peaks are relatively weak. We consistently find the following:

- appearance of an asymmetric in-plane ring deformation at 1250 cm^{-1} ($\mathscr{M}25$)
- shift of out-of-plane CH deformation ($\mathscr{M}19$) from 497 cm^{-1} at neutral and basic pH to 487 cm^{-1} at acidic pH
- change of mode $\mathscr{M}10$ (in-plane ring deformation with C-S stretching) from a double peak at 705/720 cm^{-1} to a single peak at 712 cm^{-1}
- a 10 cm^{-1} frequency increase of both protonated and deprotonated C=C stretching peaks from basic to acidic pH
- shift of an asymmetric in-plane ring deformation ($\mathscr{M}29$) from 662 cm^{-1} to 645 cm^{-1}

A recent study of individual mercaptopyridine molecules adsorbed on Au(111) in UHV by inelastic electron tunneling spectroscopy (IETS) found that out-of-pane CH bending modes between 720 cm^{-1} and 970 cm^{-1} show different spectra for molecules adsorbed in elbow or on fcc sites[42]. Accompanying DFT calculations including anharmonic interactions predicted that both out-of-plane CH deformations and modes involving the C-S stretch would shift distinctly when the pyridine ring plane tilts.

It has been suggested in the literature that H_2SO_4 plays a special role as solvent, because adsorbed pyS was found to possess different long range order and tighter packing onto a Au(111) in H_2SO_4 than in other solvents by scanning tunneling microscopy[36]. This was suggested to stem from the electrostatic attraction of SO_4^{2-} to two protonated pyridine rings in a bridging configuration, even though the STM images did not exhibit any specific features relating to adsorbed sulfate ions. Since our results from various acids fall onto the same curve in Fig. 3, we have no indication that sulfate ions create a discernible effect in the spectra.

In order to obtain a slightly deeper insight, we use density functional theory to simulate various complexes of py and pyS-Au with various hydrogen-bonding species. Since we know from experiment that the trigonal ring deformation mode does not change frequency in the different solvents (its frequency is a measure of the bond strength of pyS to the surface), we scale all calculated spectra to the experimental value of 1092 cm^{-1} for this mode. We then apply an extra scaling factor of 0.99 to the C=C stretching frequencies only to bring them into good overlap with the experimentally measured frequencies. The NIST computational database[43] shows that different scaling factors need to be employed for different pyridine vibrations. The resulting ring breathing and stretching frequencies are plotted in Fig. 5 as a function of the N-H bond length. The frequencies of deprotonated pyS-Au are included at an arbitrary N-H distance of 2.4 Å in the graph. The supporting information contains Table S2 with all results and scaling factors for the different systems. For pyS-Au, the single metal atom is enough to reproduce the main features (highest intensity for totally symmetric modes) and reproduces the experimental frequencies of pyS-Au over a wide range (supporting information Figure S4). Proton transfer occurs for N-H distances smaller than about 1.2 Å.

It can be seen in Fig. 5 that the calculated ring stretching frequencies fall into two groups - one where proton transfer has occurred and one where only a hydrogen bond exists or where the nitrogen lone pair is free. Given the broad vibrational linewidths on surfaces, this confirms why only two peaks are seen in the spectra even though we can have three types of adsorbed pyS. The overall pattern is the same as for pyridine itself (data scaled to a trigonal ring deformation frequency of 1030 cm^{-1}) and the ring stretching frequencies are remarkably similar. The dependence of the ring breathing mode on N-H distance is however more complex and the range of values is not as large in the calculations as in experiment. For both pyridine and adsorbed mercaptopyridine, we find that the protonated species have the highest frequency, although all calculated mercaptopyridine species have the same orientation of the ring plane which is almost perpendicular to the Au-S bond. We can cause an orientation change, where the ring plane becomes nearly parallel to the Au-S bond, by coordinating an additional molecule to H^+-pyS-Au. Adding a benzene molecule in a T-shaped conformation simulates a cation/π interaction between the positive charge on the pyridine ring and the benzene π system. We obtain a similar effect if we coordinate a water molecule to protonated pyridine (we calculated $H_2O\cdots H^+$-pyS-Au and H_3O^+-pyS-Au). Given that two very different molecules can produce the same effect, the key driver in the reorientation is probably simply a change in electron density near the ring nitrogen. In both cases, the ring breathing frequency decreases to values closer to bare pyS.

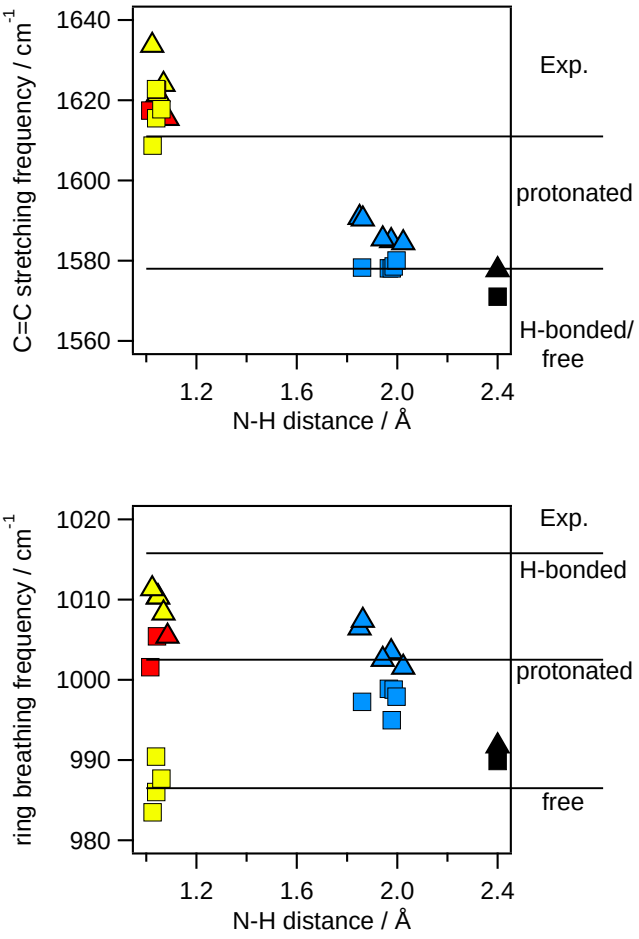

Fig. 5 DFT calculation of the ring breathing and ring stretching frequencies of hydrogen-bonded and protonated pyS-Au and py species. Squares are for pyS-Au, triangles are for py. Colour coding: black - free N lone pair; blue - H bonded to water, ethanol etc.; red - protonated species; yellow symbols are for benzene and water coordinated to a protonated pyridine ring, which causes an orientation change.

To understand why a rotation of the ring would affect the ring breathing frequency, we extracted the N-$C_{2,6}$ and $C_{2,6}$-$C_{3,5}$ bond lengths for the various calculated species (supporting information Figure S6). The hyperconjugation effect on the $C_{2,6}$-$C_{3,5}$ bonds is visible as a decrease from 1.393 Å to 1.380 Å upon protonation. Rotation of the protonated ring by coordination to benzene or water decreases this bond length further to 1.375 Å. The N-C bond length does not change with ring rotation, but the $C_{3,5}$-C_4 bond length increases from about 1.41 Å to 1.415 Å. Since the ring breathing frequency depends on all three force constants of the N-C bonds and C-C bonds[44], differences in the ring geometry could explain the unusual frequency ordering.

It therefore appears that an orientation change, possibly caused by cation/π interaction of protonated pyS with neighbouring neutral pyS or by interaction with a water molecule, is the most

likely explanation for the unusual frequency ordering. The discussion above shows that the commonly used intensity ratio of ring breathing / trigonal ring deformation is not a good measure of pH, because several species contribute to the signal. Instead, the C=C stretching intensity ratio is a better representation of pH, while deconvolution of the ring breathing peak allows to retrieve the relative fractions of free and hydrogen-bonded pyS-Au. For example, when the pH-sensitive CC stretching and CH deformation peaks are used for enantioselective detection of alcohols[12], hydrogen bonding to any alcohol would increase the so-called deprotonated peaks, not the protonated ones. This understanding will therefore help to create better sensors involving the pyridine lone pair in the future.

4 Conclusions

This work reveals that the ring breathing peak of pyS SERS spectra can be used to distinguish free, H-bonded and protonated species. The latter species has actually a lower frequency than the H bonded one despite a more aromatic ring, because cation/π or cation/water interaction probably causes an orientation change in the adsorbed molecule, which lowers the frequency. Accounting for the presence of multiple ring breathing peaks will help to paint a more complete picture of 4-mercaptopyridine as a sensor of the solvent environment.

Conflicts of Interests

There are no conflicts of interest to declare.

Acknowledgements

N.W. gratefully acknowledges Mahidol University, Thailand, and University of Liverpool, UK, for receipt of a Mahidol-Liverpool Stang Mongkolsuk PhD Scholarship. Part of this work was supported by the Leverhulme Trust (RPG-2012-632). The authors would like to thank Prof. Oren Scherman for an organic chemist's insight into cation/π interactions.

References

1 I. Taniguchi, S. Yoshimoto, M. Yoshida, S.-i. Kobayashi, T. Miyawaki, Y. Aono, Y. Sunatsuki and H. Taira, *Electrochimica Acta*, 2000, **45**, 2843–2853.

2 L. Guerrini, I. Rodriguez-Loureiro, M. A. Correa-Duarte, Y. H. Lee, X. Y. Ling, F. J. Garcia de Abajo and R. A. Alvarez-Puebla, *Nanoscale*, 2014, **6**, 8368–75.

3 T. Nankawa, Y. Suzuki, T. Ozaki, A. J. Francis and T. Ohnuki, *Journal of Nuclear Science and Technology*, 2008, **45**, 251–256.

4 F. Eberle, M. Saitner, H.-G. Boyen, J. Kucera, A. Gross, A. Romanyuk, P. Oelhafen, M. D'Olieslaeger, M. Manolova and D. Kolb, *Angewandte Chemie International Edition*, 2010, **49**, 341–345.

5 C. Silien, M. Buck, G. Goretzki, D. Lahaye, N. R. Champness, T. Weidner and M. Zharnikov, *Langmuir*, 2009, **25**, 959–967.

6 M. I. Muglali, A. Bashir, A. Terfort and M. Rohwerder, *Phys Chem Chem Phys*, 2011, **13**, 15530–8.

7 T. Shegai, A. Vaskevich, I. Rubinstein and G. Haran, *Journal of the American Chemical Society*, 2009, **131**, 14390–14398.

8 J. Hu, B. Zhao, W. Xu, B. Li and Y. Fan, *Spectrochimica Acta Part A: Molecular and Biomolecular Spectroscopy*, 2002, **58**, 2827–2834.

9 R. Jensen, J. Sherin and R. S. Emory, *Applied Spectroscopy*, 2007, **61**, 832–838.

10 K. L. Nowak-Lovato and K. D. Rector, *Int J Anal Chem*, 2012, **2012**, 390182.

11 X. S. Zheng, P. Hu, Y. Cui, C. Zong, J. M. Feng, X. Wang and B. Ren, *Anal Chem*, 2014, **86**, 12250–7.

12 Y. Wang, Z. Yu, W. Ji, Y. Tanaka, H. Sui, B. Zhao and Y. Ozaki, *Angew Chem Int Ed Engl*, 2014, **53**, 13866–70.

13 N. Yu, HZ.; Xia and Z. Liu, *Anal Chem*, 1999, **71**, 1354–1358.

14 M. Bryant and R. Crooks, *Langmuir*, 1993, **9**, 385–387.

15 T. de F. Paulo, H. D. Abruña and I. C. N. Diógenes, *Langmuir*, 2012, **28**, 17825–17831.

16 E. R. Berg, S. A. Freeman, D. D. Green and D. J. Ulness, *The Journal of Physical Chemistry A*, 2006, **110**, 13434–13446.

17 Z.-Q. Tian, B. Ren and D.-Y. Wu, *The Journal of Physical Chemistry B*, 2002, **106**, 9463–9483.

18 X. Li and A. A. Gewirth, *Journal of the American Chemical Society*, 2003, **125**, 7086–7099.

19 D. F. Yang, C. P. Wilde and M. Morin, *Langmuir*, 1996, **12**, 6570–6577.

20 J. F. Li, X. D. Tian, S. B. Li, J. R. Anema, Z. L. Yang, Y. Ding, Y. F. Wu, Y. M. Zeng, Q. Z. Chen, B. Ren, Z. L. Wang and Z. Q. Tian, *Nat Protoc*, 2013, **8**, 52–65.

21 J. Bielecki and E. Lipiec, *J Bioinform Comput Biol*, 2016, **14**, 1650002.

22 A. D. Boese, *Chemphyschem*, 2015, **16**, 978–85.

23 R. L. Birke and J. R. Lombardi, *Journal of Optics*, 2015, **17**, 114004.

24 A. M. Gardner and T. G. Wright, *J Chem Phys*, 2011, **135**, 114305.

25 H. Guo, L. Ding and Y. Mo, *Journal of Molecular Structure*, 2011, **991**, 103–107.

26 Z. Wang and L. J. Rothberg, *The Journal of Physical Chemistry B*, 2005, **109**, 3387–3391.

27 P. Singh and V. Deckert, *Chem Commun (Camb)*, 2014, **50**, 11204–7.

28 M. Bron and R. Holze, *Journal of Solid State Electrochemistry*, 2015, **19**, 2673–2682.

29 G. Niaura and A. Malinauskas, *Journal of the Chemical Society, Faraday Transactions*, 1998, **94**, 2205–2211.

30 Z. Shi, J. Lipkowski, M. Gamboa, P. Zelenay and A. Wieckowski, *Journal of Electroanalytical Chemistry*, 1994, **366**, 317–326.

31 I. V. Alabugin, M. Manoharan, S. Peabody and F. Weinhold, *Journal of the American Chemical Society*, 2003, **125**, 5973–5987.

32 A. Y. Li, H. B. Ji and L. J. Cao, *J Chem Phys*, 2009, **131**, 164305.

33 T. M. Krygowski, H. Szatyłowicz and J. E. Zachara, *The Journal of Organic Chemistry*, 2005, **70**, 8859–8865.

34 S. Tsuzuki, M. Mikami and S. Yamada, *Journal of the American Chemical Society*, 2007, **129**, 8656–8662.

35 S. M. Melikova, K. S. Rutkowski, A. A. Gurinov, G. S. Denisov, M. Rospenk and I. G. Shenderovich, *Journal of Molecular Structure*, 2012, **1018**, 39–44.

36 T. Baunach, V. Ivanova, D. A. Scherson and D. M. Kolb, *Langmuir*, 2004, **20**, 2797–2802.

37 Y. Wang, Q. Chi, N. S. Hush, J. R. Reimers, J. Zhang and J. Ulstrup, *The Journal of Physical Chemistry C*, 2011, **115**, 10630–10639.

38 T. Sawaguchi, F. Mizutani and I. Taniguchi, *Langmuir*, 1998, **14**, 3565–3569.

39 S. Herrera, F. Tasca, F. J. Williams, E. J. Calvo, P. Carro and R. C. Salvarezza, *Langmuir*, 2017, **33**, 9565–9572.

40 T. Burgi, *Nanoscale*, 2015, **7**, 15553–67.

41 J. Kucera and A. Gross, *Langmuir*, 2008, **24**, 13985–13992.

42 I. S. Ulusoy, Y. Scribano, D. M. Benoit, A. Tschetschetkin, N. Maurer, B. Koslowski and P. Ziemann, *Physical Chemistry Chemical Physics*, 2011, **13**, 612–618.

43 *NIST Computational Chemistry Comparison and Benchmark Database, NIST Standard Reference Database Number 101*, Release 18, October 2016, http://cccbdb.nist.gov/.

44 G. Mizutani and S. Ushioda, *The Journal of Chemical Physics*, 1989, **91**, 598–602.